Electrical characteristics of the oxyfuel flame while cutting steel

Teresa L. Pond, Christopher R. Martin[a,*]

[a] *The Pennsylvania State University, Altoona College, 3000 Ivyside Park Altoona, PA 16601*

Abstract

We present the first published record of electrical phenomena in the oxyfuel cutting torch flame while cutting a steel work piece. Measurements of the voltage-current characteristic between the torch and the work piece demonstrate three piecewise-linear regimes in the ±10V range. Flame resistance measurements in the ohmic regime are studied using three candidate excitation signals while varying fuel/oxygen ratio, feed rate, and standoff distance. Electrical characteristics are also observed during successful and unsuccessful pierce and loss-of-cut events. The flame's electrical resistance is found to be 2.8kΩ per mm of length; a factor of 3 smaller than the same conditions without cutting oxygen. We present an argument that the drastic increase in plasma conductivity is due to an abundance of electrons produced at the work piece. We draw preliminary conclusions about the potential applicability of these measurements for the in-process detection of standoff, pierce success, and loss-of-cut events.

1. Introduction

This work provides the first published record of the electrical attributes of the oxyfuel torch's flame during the cutting process. Motivated by shortcomings in the contemporary sensing and control technologies available, recent works [1, 2] have established attributes of the current-voltage characteristic that can be related to process parameters in a preheat configuration. In addition to providing a potentially interesting case for the validation of predictive models, these signals represent a promising alternative for the detection of important process parameters while eliminating the need for active sensing elements proximate to the process.

In the development of any sensing technology, a robust empirical description of the relevant physical phenomena is essential. Only in the past few years have measurements become available for the characteristics of the preheat flame, but ion current measurements during a cut remain conspicuously absent in the literature.

In this work, we investigate the current-voltage (IV) characteristic between the torch and work, we demonstrate a method for robustly measuring the flame's electrical resistance, and we study its behavior with respect to cut speed, standoff, and fuel/oxygen ratio during the cutting process. Because the system exhibits geometric and chemical complexities atypical of classical laboratory flame studies, we include a description of the physical process before reviewing the state of measurements represented in literature.

1.1. To the oxyfuel cutting process

Now over a century-old, oxyfuel cutting is a manufacturing technique for cutting iron and steels that has retained its relevance to contemporary manufacturing due to low costs and unparalleled performance on thick work pieces. Spurred on by the rise of total automation in the manufacturing sector, there is significant interest in the electrical aspects of the oxyfuel flame as a potential means to address the many

Figure 1: A two-piece oxyfuel cutting tip. The grid is 12.5mm (0.5in) spacing.

shortcomings of the current sensing and control technologies.

While this process could conceivably be executed with a number of geometries, torches have widely converged to adopt a consistent design. In the vast majority of all mechanized torch tips, preheat holes are arranged in a circular array around a central cutting oxygen bore as shown in Figure 1. The preheat holes supply a premixed fuel-oxygen mixture (represented as a in Figure 2) to the preheat flamelets that form inner cones on the torch tip (b). While these holes may vary in number and shape, they are sized to allow the incoming gas to cool the tip and to prevent the flame front from flashing into the torch.

The preheat flame alone is far less intense than would be required to melt away material. Instead, the process uses a jet of pure oxygen (the "cutting" oxygen) to sustain an intense oxidation reaction to burn away a void in the material called a "kerf." The heat released in that reaction combined with the preheat flame sustains the process.

The preheat flame is usually described as exhibited two major geometric features: outer and inner cones. The inner cones (b in Figure 2) are well defined intensely luminous conical sheets that anchor over the preheat holes. They are shrouded in a single faintly luminous outer cone (c), which washes over the work.

The oxyfuel cutting process is conducted in three stages that are depicted in Figure 2.

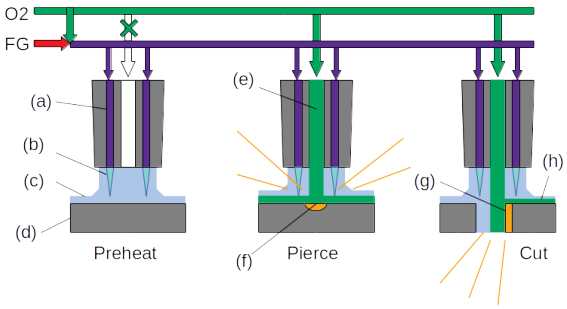

Figure 2: The three stages of the oxyfuel cutting process

1. **Preheat** A preheat flame (b,c) is used to bring a metal work piece to its kindling temperature; the temperature at which the material will auto ignite in an oxygen atmosphere. In proper use, the tip of the inner cones (b) should terminate near the work surface (d), and the outer cone (c) should wash over the work. No cutting oxygen is applied in this step.
2. **Pierce/Ignition** A jet of pure oxygen (e) is applied to the work piece to burn away material. In a "pierce" operation, the jet is applied over the work until it burns a hole (f). Alternatively, a faster and cleaner "edge start" can be executed by applying the cutting oxygen across the face of one of the work piece edges.
3. **Cutting** The oxygen jet is advanced into the material to burn (g) a kerf. Because of the continuous feed of fresh material into the jet, a portion (h) is deflected across the top of the work, causing a small but visible flux of radiating metal particulates.

The cut is stopped by halting the flow of cutting oxygen while leaving the preheat flame lit.

The difficulty in fully automating the process lies in the number of factors that are both challenging to sense and lethal to the process if incorrect. For example, if the work is not sufficiently heated prior to a pierce operation, the cutting oxygen will wash over the metal and cool it rather than igniting the steel. Similarly, if the the torch is moved too quickly during a cut operation, the feed of fresh material will depress the temperature in the kerf, and the cut can be "lost" when the work ceases to burn.

Arguably, the most critical parameters for achieving a reliable quality cut are:

1. **Feed rate**: the rate at which the torch is moved into fresh material is critical for determining the quality of cut and ensuring the reliability of the cut. It is also important that the motion be smooth; vibration or jerks in the motion of the torch are no different from rapid feeds, and can cause the cut to be lost.
2. **Standoff**: the distance between the torch tip and the work piece is usually set so the inner cone is immediately above the work. This usually maximizes the heat to the work piece, and provides enough space to reduce the probability that spatter from the process will damage the tip.
3. **Fuel/oxygen ratio**: the temperature of the flame is maximized at fuel-rich conditions (typically far above the stoichiometric ratio). The exact optimal depends on fuel, but operators are usually instructed to operate at the richest condition where the inner cone will reliably anchor on the torch tip.

Smooth motion at accurate feed rates is not a serious concern for CNC systems, but there are not currently robust methods for verifying that the ignition process has succeeded, for verifying the plate kindling temperature, nor for detecting loss-of-cut. Moreover, the prevailing technologies for detecting standoff leave room for improvement. Standoff is especially critical since the work pieces often warp during the cutting process. A typical standoff might be only 3 or 4mm (about 0.12 or 0.16in), so it is not uncommon for large work pieces to warp so severely in-process that variations in standoff compromise the cut. The torch might touch the work piece (called a "crash event," or the standoff might grow so much that the cut is lost.

1.2. To prior work relevant to the oxyfuel preheat flame

The study of ion currents in flames is a rich field of well documented investigation spanning centuries; with a flurry of major advances in the past six decades. Because the chemical ionization in flames provides one of the few opportunities to both force and measure motion of select molecules in a gas, the study of ion mobility has long been a pillar of the kinetic theory of gases [3]. By the late nineteen sixties, work on ions in flames had progressed sufficiently to enable the book by Lawton and Weinberg [4]. The findings of the twentieth century are well reviewed by Fialkov [5]. A lengthier discussion of these advances and their relevance to the oxyfuel flame can be found in [1].

In the present work, we benefit from the knowledge that the singly ionized hydronium molecule (H_3O^+) far outnumbers other positive ions, and that the electron is its most numerous negative counterparts [6, 7, 8]. Thanks to a body of work on the transport properties of hydronium and the free electron, we can estimate their transport properties [9, 10]. Substantial work has also been done to establish highly simplified models for formation and recombination of the dominant charged species in recent years [11, 12, 13, 14, 15], and these efforts continue as a topic of current research.

The development of sensing technologies has motivated similar investigations into signal-level voltage physics in aero-engines [16, 17], internal combustion engines [18, 19, 20, 13, 21], and furnaces [22, 23, 24]. Works by Speelman et al. [25] and Xiong et al. [14] have demonstrated the same semi-conducting characteristics we will describe below with one dimensional laminar flame geometries; encouraging the idea that reduced-order models may have some success in describing these physics.

Ion currents specific to the oxyfuel preheat geometry first became available in the literature quite recently [1, 2]. Tests over water cooled discs without the flow of cutting oxygen found that signal-level voltages ($\pm$10V) applied between the torch and the disc form a current-voltage (IV) characteristic forming three roughly piecewise-linear regimes, inspiring applications for sensing [26, 27, 28].

Figure 3 shows three tests in which fuel/oxygen ratio and standoff are varied. The portion of the characteristic including the zero-current crossing (regime 2) was dubbed the ohmic regime, and was shown to vary its slope repeatably and linearly with stand-

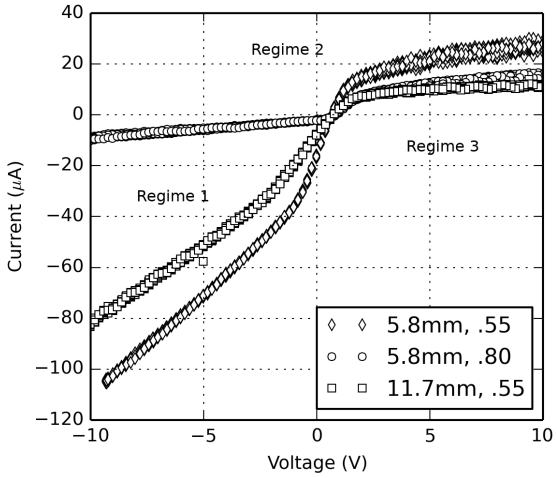

Figure 3: Current-voltage characteristics in three preheat configurations over cooled steel.

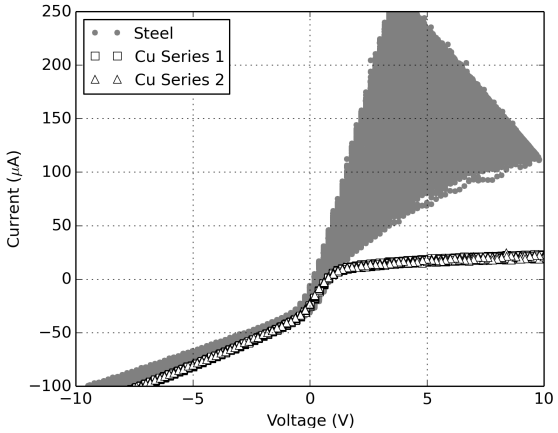

Figure 4: Current-voltage characteristics over cooled copper and over salt-coated steel with all other conditions equivalent.

off distance. The slope in regime 1 was shown to be influenced repeatably by both standoff and the fuel/oxygen ratio. The current at which the transition between regime 1 and regime 2 occurs was determined to depend only on the fuel/oxygen ratio. In tests over a reducing substance like iron, currents in regime 3 were not found to be repeatable even when controlling surface temperature and duration of test. Over copper (which benefits from a stable oxide layer), regime 3 was found to be a repeatable indication for the arrival of positive ions at the disc surface, and utterly independent of the disc diameter or temperature.

These findings have invited the conclusion that the oxyfuel flame exhibits two major sources of ions:

- **primary ions** generated in the inner cone, where hydronium and (mostly) electrons are generated by well established kinetic models, and
- **secondary ions** generated by chemical action at the work surface.

As is implied by the monikers *primary* and *secondary*, primary ions have been found to dominate secondary in the preheat flame, but the addition of salts to the work surface have already shown that this is not necessarily always the case [2]. Figure 4 shows the current-voltage characteristic measured over copper and salt-coated steel under the same conditions. The readily ionized salts at the work surface enhance the regime 3 currents tenfold, subtly shifts the floating potential, and makes no other detectable impacts.

Since ion currents in the oxyfuel flame in a cutting configuration have not been published, we are left to speculate that the intense redox reaction in the kerf will strongly impact regime 3 as did the salts in Figure 4. The present effort is designed to address this deficit in the literature and to establish what (if any) phenomena may be unique to the cutting configuration.

2. Approach

2.1. To the experiment

Measurements were conducted using an ESAB Silhouette 500 cutting machine modified for digital control, with a C-67 oxyfuel torch burning industrial grade methane (95% pure) and oxygen. Low-speed two-piece 1/2-inch tips were used to cut 12.7mm (0.5in) low carbon steel (ASTM A572) samples, as shown in Figure 5. The gas hoses were electrically isolated with PTFE polymer threaded adapters, and

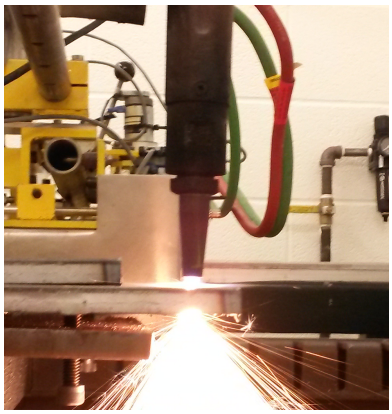

Figure 5: The experiment during a constant-standoff cut.

the torch mount was isolated with layers of Nomex approximately 1.5mm (.06in) thick.

Preheat fuel gas and oxygen were metered using the system described in [1]. The flow rate of fuel gas and oxygen were monitored using thermal mass flow meters throughout the tests, and adjusted using precision needle valves at a control panel in a separate room from the test; ensuring stable gas flow rates throughout the experiment. The preheat and cutting oxygen lines were supplied from a common bottle, but through separate station regulators to isolate the preheat oxygen from fluctuations as the cutting oxygen was switched on or off. As is typical of oxy-fuel cutting processes, the cutting oxygen pressure (rather than flow rate) was monitored.

Tests were conducted by performing linear cuts in one of three configurations:

1. **Constant tests** These cuts were conducted while holding feed rate and standoff distance constant throughout the cut. Heights from 2.5mm (0.1in) to 7.5mm (0.3in) in 1.25mm (0.05in) increments were studied in this manner.
2. **Inclined tests** These cuts were conducted while holding the feed rate constant over a deliberately inclined plate so that the standoff distance may be presumed to change linearly throughout the cut.
3. **Feed tests** These cuts were conducted while holding the standoff distance constant, but while changing the feed rate through a schedule of speeds.

Most tests were 300mm (12in) long drop cuts (edge-to-edge), but some tests were on shorter lengths, and some were executed in a pierce configuration.

In all tests, the work piece was placed on three points of contanct with adjustment screws below (two of which are visible in Figure 5). Prior to each cut, gauge blocks were used to establish the distance between the torch and the work at the beginning and end of the cut path, and the screws were iteratively adjusted until the plate achieved the desired level(s) throughout the cut. In most tests, the height was re-verified after the cut to check for motion of the plate.

An analog amplifier circuit described in [2] was employed to supply signals of constant-current or constant voltage to the torch relative to the grounded work. A LabJack T7 data acquisition device supplied an analog command to the amplifier while monitoring feedback signals indicating both torch voltage and current in all configurations. The amplifier was recalibrated prior to these tests, and the current feedback calibration was found to be accurate to within 0.2μA with 100kΩ and 1MΩ loads, tested at currents in the range $\pm 100\mu$A. The buffered voltage measurement was found to be within 5mV of the actual voltage over the range $\pm$12V.

2.2. To electrical excitation

Establishing precise measurements of the IV characteristic slope in the ohmic regime is one of our highest priorities in these measurements. This slope represents the total electrical resistance of the flame when currents are slight enough that no emitting surface has been driven to saturation. As a result, the quantity of charged species and their mobility in the bulk of the flame are the only limiting physical properties that determine current.

Electical excitations were conducted in two stages. First, $\pm$10V triangle waves were applied to establish the form of the IV characteristic for the torch in the cutting configuration. In previous works [1, 26, 27, 28], these were then fit by an iterative piecewise-linear regression algorithm to obtain the

slopes and intercepts of each of the regimes. However, in a cutting configuration, the measurement is complicated by unsteady phenomena that might produce a point cloud similar to Figure 4, so that a more specialized technique is called for.

Since the narrow range of voltages spanning the ohmic regime can be shifted by chemical action at the work surface (see the horizontal scatter in Figure 4) current excitaitons should be applied while voltages are monitored to ensure that the measurements remain in regime 2. If efforts to remain in the linear region are successful, then the voltage may be expected to adopt the behavior

$$V = V_0 + R_2 I + V_n, \tag{1}$$

where V_0 is the floating potential, R_2 is the ohmic regime resistance, and V_n represents an amalgamation of electrical noise and all other sources of uncertainty in the voltage not influence by the flame resistance or the applied current.

We address the complicating factors of the floating potential and noise simultaneously by applying a current excitation with some frequency, f, some amplitude, I_a, and some offset, I_o,

$$I(t) = I_a \cos(2\pi f t) + I_o. \tag{2}$$

The Fourier transform of the voltage signal would then be

$$\mathcal{F}\{V\}(f) = \mathcal{F}\{V_0\}(f) + \mathcal{F}\{R_2 I\}(f) + \mathcal{F}\{V_n\}(f). \tag{3}$$

If the following constraints are respected

1. the signal remains in the ohmic regime so that Equation 1 remains valid,
2. the signal is accumulated over a sufficiently short period that R_2 and V_0 may be regarded as constant,
3. the portion of the V_n energy at frequency, f, is small, and
4. the excitation frequency, f, is sufficiently low that capacitive and inductive effects are irrelevant,

then $0 = \mathcal{F}\{V_0\}(f) \approx \mathcal{F}\{V_n\}(f)$, and

$$R_2 = \text{real}\left(\frac{\mathcal{F}\{V\}(f)}{\mathcal{F}\{I\}(f)}\right). \tag{4}$$

This method for rejecting DC and noise sources is fundamentally identical to the method employed by lock-in amplifiers.

2.3. To verifying signal integrity

The simplest means of verifying the integrity of such a measurement is to repeat it while varying the excitation amplitude and offset. While the amplifier was capable of measuring currents up to $\pm 250\mu$A, it only accepted current commands up to $\pm 25\mu$A. Three sinusoidal current excitations were employed in the study of the ohmic regime resistance: 0-25μA, 0-10μA, and 5-15μA at 10Hz. If these measurements can be shown to be self-similar at comparable conditions, then the measurement may be interpreted as linear.

Additionally, by inspecting other frequencies in the spectrum, we can even quantify the impact of non-ideal effects. For example, if the excitation were to drift outside of the ohmic regime, a nonlinearity may appear, so that

$$V(t) = V_0 + R_2 I + aI^2 + \dots \tag{5}$$

When I is a cosine, I^2 will cause the appearance of a super-harmonic which would not otherwise be present in the data,

$$\begin{aligned} I^2 &= (I_o + I_a \cos(2\pi f t))^2 \\ &= {I_o}^2 + \frac{{I_a}^2}{2} + 2 I_o I_a \cos(2\pi f t) + \frac{{I_a}^2}{2}\cos(4\pi f t) \end{aligned} \tag{6}$$

Similar expansions may be used to demonstrate how cubic and higher order terms can make higher super-harmonics appear, but if the nonlinearity is slight, these terms will decline rapidly in amplitude. Therefore, we may predict that the voltage response would be

$$\begin{aligned} V(t) =& V_0 + a{I_o}^2 + \frac{a}{2}{I_a}^2 + \dots \\ & I_a(R_2 + 2aI_o)\cos(2\pi f t) + \dots \\ & \frac{a}{2}{I_a}^2 \cos(4\pi f t) \end{aligned} \tag{7}$$

when cubic and higher order nonlinear terms are neglected.

The measured resistance would, therefore, be

$$R_{meas} = \frac{\mathcal{F}\{V\}(f)}{\mathcal{F}\{I\}(f)} = R_2 + 2aI_o. \tag{8}$$

Since the coefficient, a, is not known, we would need to estimate the error by inspecting the magnitude of the super-harmonic.

$$\frac{\mathcal{F}\{V\}(2f)}{\mathcal{F}\{I\}(f)} = \frac{a}{2} I_a \tag{9}$$

Therefore, the resistance measurement error due to nonlinearity, δR, might be approximated by

$$\delta R \approx 2aI_o = \frac{4I_o}{I_a} \frac{\mathcal{F}\{V\}(2f)}{\mathcal{F}\{I\}(f)}. \tag{10}$$

Finally, the error as a fraction of the measurement can be found from the ratio of Equations 10 and 8,

$$\frac{\delta R}{R_{meas}} \approx \frac{4I_o}{I_a} \frac{\mathcal{F}\{V\}(2f)}{\mathcal{F}\{V\}(f)}. \tag{11}$$

It is important to note that this method for error analysis presumes that the nonlinearity is slight enough that cubic and higher terms are not present and that the current excitation contains no similar superharmonics. If either of these estimates is violated, it is no longer feasible to make a quantitative estimate from the superharmonic amplitude alone.

Similarly, if R_2 were not a constant, but a signal with its own frequency content, f_r, and phase, ϕ_r, then

$$\begin{aligned} R_2 I &= [R_o + R_a \cos(2\pi f_r t + \phi_r)]\,[I_o + I_a \cos(2\pi f t)] \\ &= R_o I_o + \dots \\ &\quad R_o I_a \cos(2\pi f t) + \dots \\ &\quad R_a I_o \cos(2\pi f_r t + \phi_r) + \dots \\ &\quad \frac{R_a I_a}{2} \cos(2\pi (f + f_r) t + \phi_r) + \dots \\ &\quad \frac{R_a I_a}{2} \cos(2\pi (f - f_r) t - \phi_r). \end{aligned} \tag{12}$$

Here, we see the appearance of beat frequencies, $f - f_r$ and $f + f_r$, which would appear as side bands symmetrical about f when $f_r < f$. If R_2 were to contain many frequencies up to f_r, a similar expansion would show a collection of terms spanning side band region from $f - f_r$ to $f + f_r$. This would appear like peak-broadening. We may detect it by inspecting the voltage frequency content at frequencies adjacent to the fundamental.

This possibility is real since unsteady phenomena are certain to occur in the kerf which may imapct the ion concentrations, turbulence intensity, and other transport phenomena. While interesting, we need derive no error estimate since, as Equation 12 shows, the fundamental frequency amplitude is still proportional to the mean resistance, R_o.

3. Results

3.1. Of current-voltage characteristic measurements

IV characteristics were collected by applying a 5Hz ±10V triangle wave to the torch with current and voltage samples collected once per millisecond. Cutting oxygen was supplied at 3.4bar (50psig). The preheat flame was provided a 0.71 fuel/oxygen ratio with 12L/min (25scfh) total flow.

For these qualitative measurements, the 300mm (12in) long plates were inclined with sheet metal shims to achieve a steeper incline than would have been achievable with the three-point leveling method described above. The cut was started at a 2.5mm (0.1in) standoff and concluded in excess of 10mm (0.4in) standoff.

Figure 6 shows current and voltage at five intervals throughout a 254mm/min (10ipm) cut. Thirty seconds into this test, the torch was preheating the leading edge of the plate in preparation for an edge start. The curve is quite similar to the preheat tests already observed over steel in previous tests.

Thirty five seconds into the test, the cut had been initiated, and the black diamonds can be seen to saturate the amplifier before there is any evidence of saturating the work. Furthermore, in comparison to the preheat signal, the slope of the ohmic region has been increased (the R_2 resistance has decreased), and the floating potential is also decreased.

Sixty five seconds into the test, the test was half complete, and the standoff had grown to 6.4mm

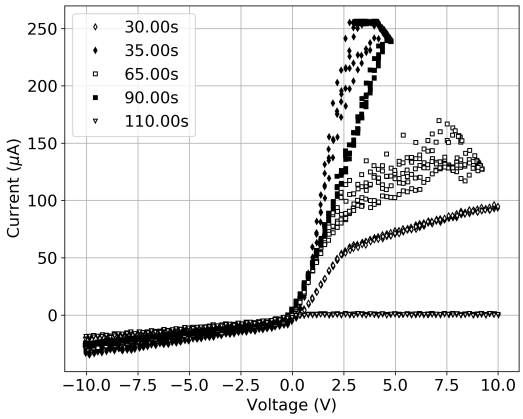

Figure 6: Current-voltage characteristics extracted from an inclined cut at 254mm/min. 30s: preheat, 35s: cutting (small standoff), 65s: near loss-of-cut, 90s: cutting (larger standoff), 110s: cut complete.

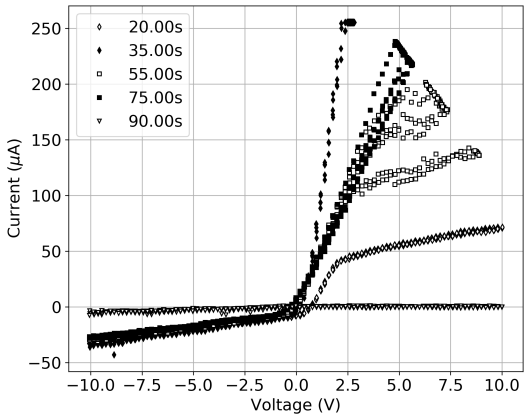

Figure 7: Current-voltage characteristics extracted from an inclined cut at 360mm/min. 20s: preheat, 35s: cutting (small standoff), 55s: near loss-of-cut, 75s: cutting (large standoff), 90s: cut complete

(0.25in). The work saturation dropped precipitously and the ohmic slope declined (resistance increased). This phenomenon persisted through the rest of the cut. The work saturation current could be seen to oscillate between the amplifier maximum at 250μA and levels around 125μA over intervals approximately five seconds long. These dynamic swings of the work saturation current appear to correspond to near-loss-of-cut events as the inner cones withdrew from the plate due to the increased standoff.

Ninety seconds into the test, the cut is nearly complete and the standoff has increased by a factor of four. In the data shown, the IV characteristic had momentarily recovered its original shape, and the decline in slope (increase in ohmic regime resistance) is immediately obvious next to the data at thirty five seconds.

Figure 7 shows a test with identical conditions, but with a feed rate of 356mm/min (14ipm). The results were nearly identical. The conditions are as follows: (20s) preheat, (35s) cut at 2.5mm (0.1in) standoff, (55s) about 5.5mm (0.22in) standoff, (75s) near end-of-cut and 10mm (0.4in) standoff, (90s) after end-of-cut.

Figure 8 shows data taken from a third test conducted at 467mm/min (18ipm), during which the cut was lost fifty one seconds into the test. In this test, the data at twenty seconds show the preheat IV characteristic shortly prior to the application of cutting oxygen. Fifty seconds into this cut, the work saturation current is still above the amplifier's capacity, but there was a dramatic descent in regime 3 current as the cut is lost by fifty two seconds. First, the data fall back to their levels during preheat, but then the entire positive characteristic nearly vanishes as the torch moves over a cold plate.

The onset of the intermittent drops in regime 3 current were confirmed near 6.4mm (0.25in) standoff in all three tests. At this height, the inner cones have just begun to withdraw from the work. This is consistent with the expectation that the regime 3 saturation current is an indicator for the chemical action in the kerf. Data that were plotted during one of these drops causes the cloud of data found at sixty five seconds in Figure 6, at fifty five seconds in Figure 7, or fifty two seconds in Figure 8.

3.2. Of a study on excitation methods

Figure 9 shows a brief segment of the raw current and voltage measurements during cuts while employ-

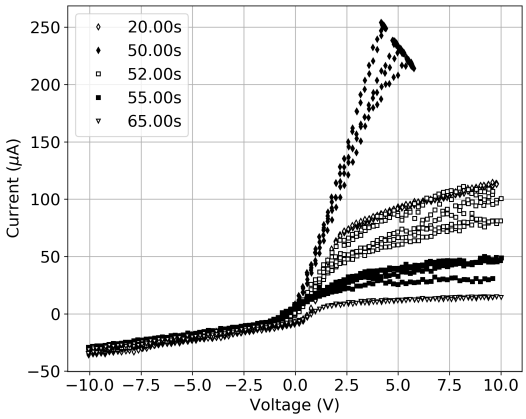

Figure 8: Current-voltage characteristics extracted from a test during loss-of-cut. 20s: preheat, 50s: cutting, 52s: loss-of-cut event, 55s: cut lost, 65s: torch over cold plate

ing the three candidate current excitations; 0-25μA, 0-10μA, and 5-15μA. From the raw current signal, it is apparent that the largest current excitation suffered a minor saturation at the top limit of the amplifier's range. In both the 0-25μA and 0-10μA tests, there is also some evidence of asymmetry between the maximum and minimum of the largest signal.

To gain insight into how these data were collected and analyzed, we first examine the data collected from three constant height cuts in some detail. These cuts were performed with a preheat flow rate at 12±0.2L/min (26±0.5scfh) and a f/o ratio 0.78±.01, with cutting oxygen pressure 3.4±0.3bar (50±5psig), and with a feed rate of 305mm/min (12ipm).

Figure 10 shows waterfall diagrams for the same three tests. The color scale is generated from the logarithm of voltage amplitude so that small signals will be easy to distinguish from the noise floor. In the initial and final seconds of the tests, there were no valid data when the flame was not in contact with the plate. The voltage signal shows clear indications of the preheat, ignition, and cut stages. In these tests, the torch was manually positioned in preheat for an edge start. After a lengthy (40s or more) preheat time, the cutting oxygen was initiated, and the torch was allowed to dwell for 2s before it was advanced at

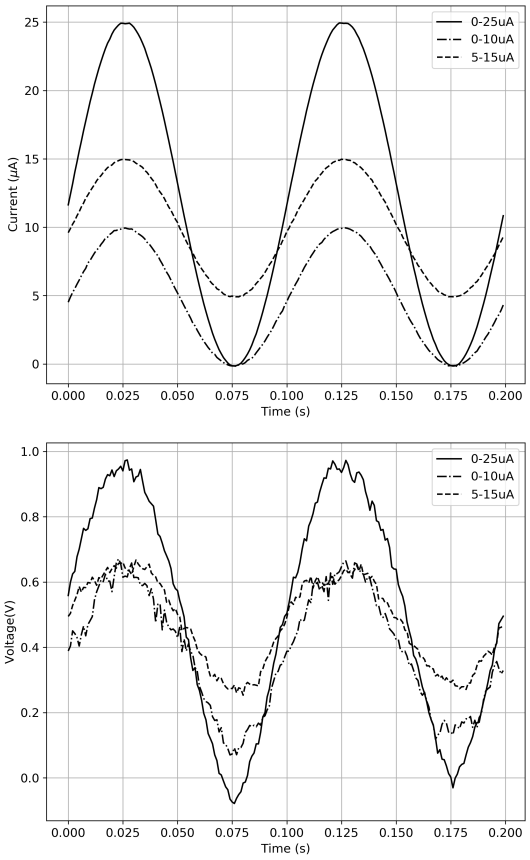

Figure 9: Three candidate current excitation signals and their resulting voltage signals during a cut.

305mm/min.

In Figure 10b, the cut began around 80s into the test, and in (d) and (f) the cuts began between 40 and 50s. In (d) and (f), there are clear events corresponding to the start of ignition and the 2s dwell as the cut was initiated. In all three tests, there is a clear dominant line at the 10Hz excitation. There are faint lines in the voltage signal corresponding to 60Hz line noise, and an acoustic resonance in the torch and its first super-harmonic around 160Hz and 320Hz (faintly audible during tests). All tests also exhibit some faint frequency content near or above 400Hz that was never definitively identified; it could be a second mode of acoustic resonance.

All voltage data exhibit strong signs of nonlinearity prior to the start of cut; the first two or three superharmonics at 20, 30, and 40Hz appear strongly. The appearance of 10Hz-interval side bands around the 160Hz resonance also provides strong evidence of nonlinear interaction between the signals. These resistance measurements should be ignored prior to ignition.

After ignition, the first two (0-25μA and 0-10μA) tests show superharmonics in the voltage data that seem to be indicators of nonlinearity, while the 5-15μA signal appears clean. However, when we inspect the current excitation signals, we find that the amplifier saturation may be to blame for the appearance of superharmonics in the 0-25μA signal while the two smaller current signals appear to have clean frequency content.

Figure 11 shows the fundamental and first two superharmonic amplitudes in calibrated voltage units. While the harmonics are clearly non-zero, they have descended into the noise floor, so that no coherent signal is apparent. The fundamental exhibits small fluctuations throughout the test, but no major characteristics. This represents a clean measurement.

3.3. Of cuts with constant conditions

These data were collected with a preheat flow rate at 12±0.2L/min (26±0.5scfh), a fuel-to-oxygen ratio 0.78±.01 by volume, cutting oxygen pressure 3.4±0.3bar (50±5psig), and with a feed rate of 305mm/min (12ipm). All cuts were initiated in an edge-start condition, and data collection continued beyond the end-of-cut. Standoffs were tested from 2.5mm (0.1in) to 7.6mm (0.3in) in 1.3mm (0.05in) increments. Most cuts were 300mm (12in) long, but some were shorter (around 150mm or 6in). Each cut severed a drop piece roughly 12 to 25mm (0.5 to 1in) wide.

Prior to each test, the height was verified using gauge blocks between the torch and work at the beginning and end of the cut line. After most cuts, the height was re-verified with calipers while the plate was still hot. Four out of forty two tests in this configuration were rejected because of clear evidence that the plate had moved during the test. Typical measurements showed about 0.5mm (.020in) of motion (believed to be due to thermal stresses in the plate).

Prior to aggregating the data, a figure like Figure 11 was examined manually for each cut. The time of the cut start and end were noted, and statistics were accumulated beginning four seconds into the cut to ensure that the torch was fully over the plate and that any transients from ignition had decayed. For each cut, the resistance mean and noise amplitude over the course of the cut was calculated as

$$R_{mean} = \frac{1}{t_1 - t_0} \int_{t_0}^{t_1} R(t) \mathrm{d}t \tag{13}$$

$$\begin{aligned} {R_{noise}}^2 &= \frac{1}{t_1 - t_0} \int_{t_0}^{t_1} \left(R(t) - R_{mean}\right)^2 \mathrm{d}t \\ &= {R_{rms}}^2 - {R_{mean}}^2. \end{aligned} \tag{14}$$

The resistance noise values bore no apparent correlation to the standoff height. A histogram of resistance "noise" levels for each of 42 cuts is shown in Figure 12. While there were several outliers with stronger variations, the vast majority of data exhibited unsteady signal content at 2.7kΩ or below. Since resistance was measured by FFT in 0.5 second windows, only low-frequency variations were not inherently rejected by the analysis. While coherent structures were not apparent, the deviations reported here represent timescales 1 to 10 seconds, corresponding to as much as 50mm (2in) of travel.

For the 0-25μA signals the magnitudes of the first harmonics were 5-10% of the fundamental, suggesting that as much as 20 to 40% error in resistance was

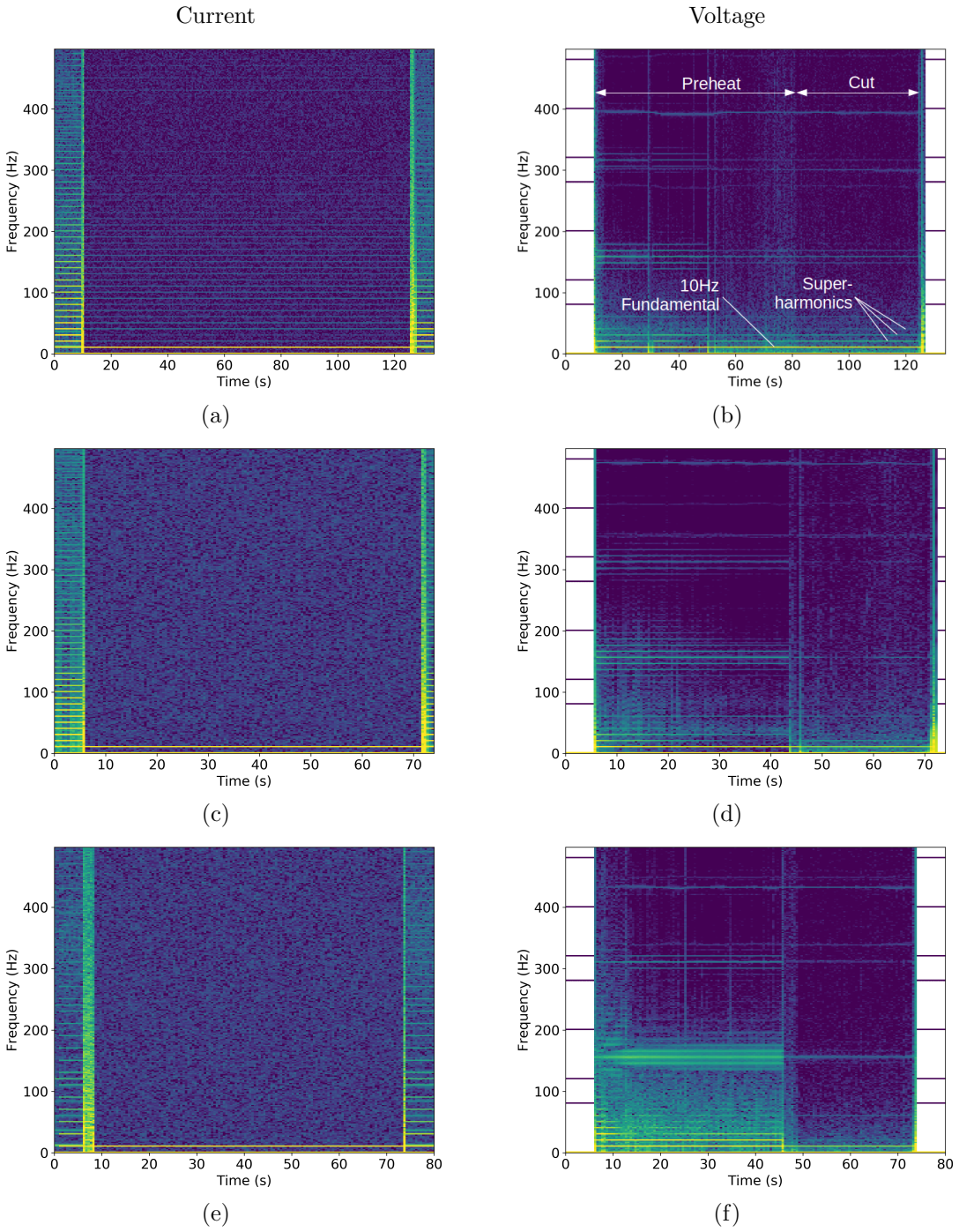

Figure 10: Waterfall diagrams for the current and voltage signals with the three candidate excitations: (a & b) 0-25μA (c & d) 0-10μA (e & f) 5-15μA

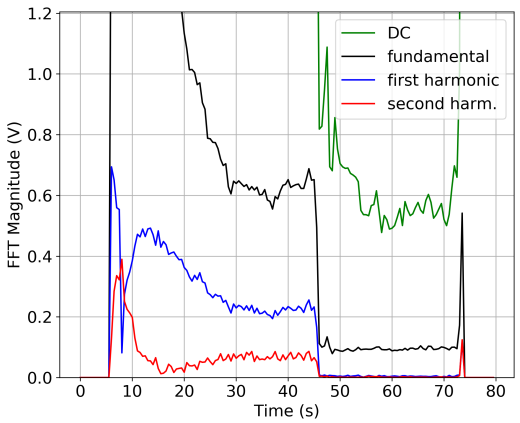

Figure 11: DC, fundamental, and first and second harmonics throughout a 5-15μA test.

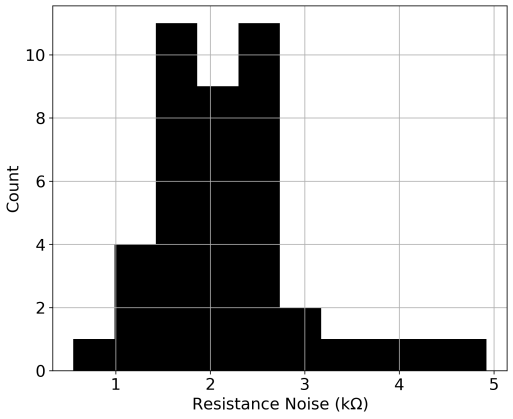

Figure 12: Histogram of ohmic regime resistance standard deviation over 42 constant-condition cuts.

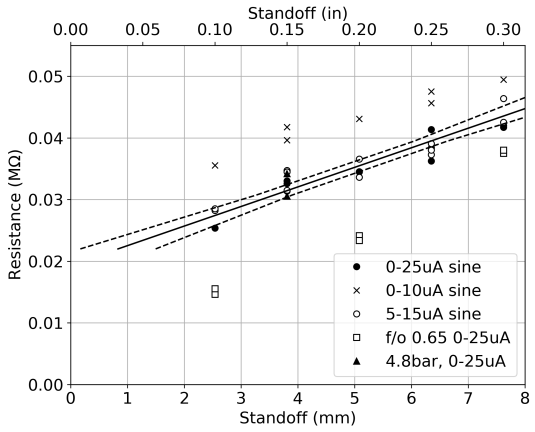

Figure 13: Mean ohmic regime resistance versus standoff under various conditions.

possible (see Equation 11). Tests with a 0-10μA excitation exhibited a first harmonic on the order of 5 to 15% of the fundamental, predicting errors as high as 60%. Meanwhile, coherent superharmonics were not identified for 5-15μA tests.

Figure 13 shows the mean resistances plotted against standoff. The three candidate signals produce data appearing in two groups; 0-25μA and 5-15μA forming one group, and 0-10μA forming a second group elevated by about 8kΩ. These observations are consistent with the errors predicted by the harmonic measurement and Equation 11.

Since harmonics are absent from data collected with a 5-15μA signal and strong in the 0-10μA data, the nonlinearity seems to be in the 0-5μA range. While the same nonlinearity would also impact data collected with a 0-25μA excitation, its impact would be reduced by a factor of 2.5. Furthermore, the presence of harmonics in the 0-25μA current signal invalidate the estimates for nonlinear error. We conclude that nonlinearity errors in the 0-25μA data are on the same order or smaller than the scatter in the data.

To quantify the sensitivity to f/o ratio while cutting, data were also collected with f/o ratio reduced to 0.65. These data show a reduction in regime 2 resistance consistent with prior measurements taken in the preheat configuration [1]. Ohmic regime re-

sistances in leaner flames (lower f/o ratio) seem to extrapolate to zero resistance at zero standoff.

To quantify the impact of cutting oxygen pressure, tests were also conducted with 4.8bar (70psig) cutting oxygen pressure. These tests were indistinguishable from the nominal 3.4bar (50psig) tests; so they were folded into the 5-15μA data set. The leaner f/o ratio decreased the resistance measurement in a manner quite similar to tests conducted entirely in the preheat configuration [1].

Table 1 provides the results of a forward and reverse linear fits of the form

$$R(s) = as + b \tag{15a}$$
$$s(R) = cR + d \tag{15b}$$

in metric and US customary units. The regression was performed using both 0-25μA and 5-15μA data, and intervals on the fits were established for a 95% confidence interval. The fit for $s(R)$ and its confidence interval are shown in Figure 13. The confidence interval for the fit and confidence intervals for the coefficients in Table 1 were established from the covariance matrices in Table 2. The fit confidence interval is produced from its variance, given calculated from equations

$$\mathrm{var}[R(s)] = s^2\mathrm{var}(a) + 2s\,\mathrm{cov}(a,b) + \mathrm{var}(b) \tag{16a}$$
$$\mathrm{var}[s(R)] = R^2\mathrm{var}(c) + 2R\,\mathrm{cov}(c,d) + \mathrm{var}(d). \tag{16b}$$

Table 1: Resistance and standoff regression results with 95% confidence intervals

	a	
2.791 53	±0.428 75	kΩ/mm
70.904 9	±10.890 25	kΩ/in
	b	
21.300 1	±2.289 6	kΩ
	c	
314.999	±48.381	mm/MΩ
12.401 5	±1.904 7	in/MΩ
	d	
-6.096 54	±1.732 90	mm
-0.240 021	±0.068 242	in

Table 2: Regression covariance matrices

	a (kΩ/mm)	b (kΩ)
a	0.050 921 84	-0.258 683 0
b	-0.258 683 0	1.452 091
	c (mm/MΩ)	d (mm)
c	648.389 2	-23.005 60
d	-23.005 60	0.831 835 4

3.4. Of cuts while varying speed

To establish the experimental sensitivity to cutting speed, data were collected while varying the cutting speed through a schedule of feed rates. For comparison to previous data, these tests were executed with the same conditions as the constant-condition tests: preheat flow rate at 12±0.2L/min (26±0.5scfh), f/o ratio 0.78±.01, and cutting oxygen pressure 3.4±0.3bar (50±5psig).

Speeds were adjusted every 50.8mm (2in) of cut through the sequence 254mm/min (10ipm), 356 (14), 406 (16), 305 (12), 203 (8), and 152mm/min (6ipm). Tests were conducted twice at 2.5mm (0.1in) and 6.4mm (0.25in) standoffs using 0-25μA excitations.

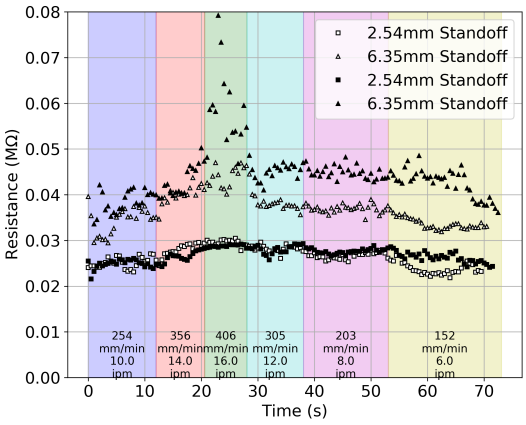

Figure 14: Ohmic regime resistance while varying feed rate.

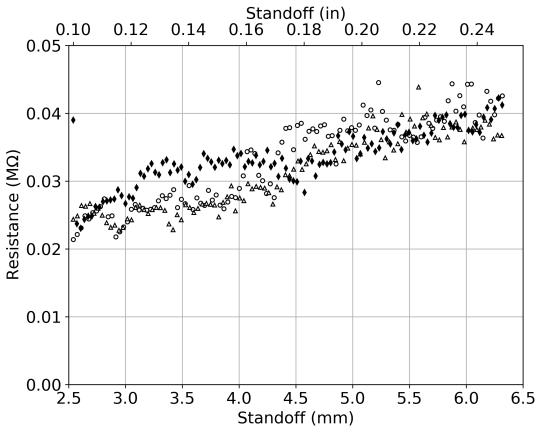

Figure 15: Ohmic regime resistance while cutting inclined plates.

Figure 14 was produced by calculating the times at which the 2-inch segments were complete. These data exhibit a small rise in resistance with increasing speeds at low standoff, but a severe dependency at a higher standoff.

3.5. Of cuts on inclined plates

To illustrate both repeatability and signal versus noise in the resistance measurements, three tests were conducted with a 0-25μA excitation over 300mm (12in) plates that were deliberately inclined to produce cuts from 2.5mm (0.1in) to 6.4mm (0.25in) standoff. For comparison with the previous tests, they were conducted with a preheat flow rate at 12±0.2L/min (26±0.5scfh), a fuel-to-oxygen ratio 0.78±.01 by volume, cutting oxygen pressure 3.4±0.3bar (50±5psig), and with a feed rate of 305mm/min (12ipm).

In Figure 15, the three tests are over-plotted with the x-axis re-scaled to reflect the nominal standoff at that point in the cut. The tests with white markers were conducted on the same plate and on the same day. The test with black markers was conducted on a different plate on a different day.

4. Discussion

4.1. Of the zero-standoff resistance

When the resistance fit established in Figure 13 is extrapolated to zero standoff, the flame resistance can be said with confidence not to approach zero. This counter-intuitive finding was also discovered in the study of the preheat flame [1]. This offset vanishes as the f/o ratio reduces, so it was originally attributed to a deficit in the production of ions at some location in the flame. Because it affects the offset and not the slope, the effect must be localized to the tip of the torch. [26] attributed this to an effective "inner cone resistance" that grows as the cones elongate and eventually lift from the torch under rich conditions. The data here are still consistent with this explanation.

4.2. Of the flame's resistance

These measurements indicate that 2.8kΩ are gained for every mm of standoff. Confidence intervals for the fit dictate that this could be as high as 3.2kΩ/mm or as low as 2.4kΩ/mm. For the same torch, values established for the preheat flame without the flow of cutting oxygen over both reactive and non-reactive work pieces have been demonstrated to be about 7.8kΩ/mm [1, 2]. Therefore, we find that

while cutting, the flame has roughly one third of its electrical resistivity during preheat.

To assign cause for this change, we must examine the mechanisms for ion transport in the flame: convection with the bulk flow, diffusion, and the electrical mobility. Of all of these, electrical mobility is the only one that responds to the external electric field, so while diffusion and convection may contribute to floating potential, the ohmic regime resistance must be due to the finite mobility of ions in the fluid. In one dimension, the current density, J, due only to an external electric field is given as a sum of the motion of all ions,

$$J = -\frac{\mathrm{d}V}{\mathrm{d}x}\sum_k q_k \mu_k n_k. \tag{17}$$

Here, q_k, μ_k, and n_k are the charge, electrical mobility, and number density of ion species k.

The mobility of hydronium was measured in a flame by Bradley and Ibrahim [9] to be $0.82 \times 10^{-3}\mathrm{m}^2/\mathrm{Vs}$ in 1730K atmospheric flames, so we may scale it to $1.08 \times 10^{-3}\mathrm{m}^2/\mathrm{sV}$ in a 3000K flame using a $\sqrt{T}$ scaling law for mobility.

The electron's mobility in ambient pressure flames was demonstrated in early measurements to be between 0.3 and $0.6\mathrm{m}^2/\mathrm{Vs}$ [29]. Contemporary estimates place the electron mobility around $0.4\mathrm{m}^2/\mathrm{Vs}$ with very little sensitivity to temperature [10]. The electrons benefit primarily from being 35,000 times lighter than hydronium; but they are also smaller in collisional cross-section and they are known to remain at non-equilibrium temperatures in plasmas. Even if ions of oxygen and other heavy molecules were so numerous as to equal the number of electrons, they would never hope to match the electron's mobility.

In total, therefore, in the ohmic regime, where no ion has yet been evacuated from the regions of the flame (saturation has not occurred), the resistance is dependent entirely on the mobility and abundance of electrons. The electrical resistance, R, per unit length, x, of a uniform plasma with cross section, A, a number density of charged species, n, with electrical mobility, μ, is given by

$$\frac{\partial R}{\partial x} = \frac{1}{A\mu n e} \tag{18}$$

when e is the elementary charge.

Ion number densities in the preheat flame (without cutting oxygen) were estimated to be on the order of 7×10^{16} per cubic meter [2] based on the arrival of positive ions at the work in saturation. If we were to adopt $\mu = 0.4\mathrm{m}^2/\mathrm{Vs}$, the number density of electrons to match the $7.8\mathrm{k}\Omega/\mathrm{mm}$ measured flame resistance per length would be 2.5×10^{16} per cubic meter; the correct order of magnitude and consistent to within the crude precision of the original estimate.

To form a hypothesis for the reduced resistance in the flame while cutting, we are forced to accept either that the mobility of the electron has somehow improved by a factor of three, or that the electron population in the outer cone has tripled. We might argue that the onset of intense turbulence with the addition of the cutting oxygen jet could enhance electrical mobility as turbulence is known to enhance diffusion. Turbulent diffusion can be estimated by the Taylor velocity and length scales, $D_T \approx \hat{u}l$ [30, p.500], which may be so large as 50m/s and 2mm for the present system. If we were to apply the Einstein relation to approximate an equivalent enhanced electrical mobility, we might speculate that

$$\begin{aligned}\mu_T \approx & \frac{D_T e}{kT} \\ = & \frac{\hat{u}le}{kT}\end{aligned} \tag{19}$$

when k is the Boltzmann constant. For a 3000K flame, this would correspond to a mobility around $0.4\mathrm{m}^2/\mathrm{Vs}$; certainly the correct order of magnitude.

Still, there are a number of serious problems for this proposal. Firstly, it fails to explain why resistivity rises abruptly as the cut is lost in Figures 14 and 8. Furthermore, changes in flow rate, irregularities in the work piece or the tip, cutting oxygen pressure, or any other experimental factor that enhances turbulence should have a strong impact on the flame's resistivity, but none has been recorded in this or any other study [1, 2].

On the other hand, we have already established that chemical action at the work piece provides a second source for ions, that the regime 3 saturation current is an indication for their concentration at the work surface, and that the regime 3 current rises

sharply when cutting initiates. When preheating a chemically inert work surface, the regime 3 currents were found to be approximately 25μA at comparable conditions to those in [2]. When cutting, those were found to rise more than ten fold, indicating that positive ions are abundant near the work. We would only need to accept that a small fraction of their negative counterparts are electrons that have diffused into the body of the preheat flame to modify the flame's resistivity.

To provide a preliminary test for this hypothesis, we performed two additional tests: (1) a pierce operation (not an edge start), and (2) a failed pierce operation. To cause the pierce operation to fail, the cutting oxygen was initiated with insufficient preheat time so that the plate was still quite cool. In both tests, the cutting oxygen flow field would have been the same, but the presence or absence of ions generated at the work surface will be the only variable.

Figure 16 shows the DC component, fundamental, and first two superharmonics in response to a 0-25μA excitation during a successful pierce operation. Near 177 seconds, the cutting oxygen was activated, and all components (including DC) tend rapidly to zero until the jet has penetrated the plate. Figure 17 shows the same operation over a cold plate. Here, the power supply was unable to drive the excitation, and the signals simply saturated at +10V, giving the false impression that the frequency content was zero. This semi-infinite resistance began when the cutting oxygen was initiated and persisted until it was turned off around 78 seconds.

The dissimilarity between these tests is not subtle. The presence of chemical action at the work surface lead to a drastic reduction of flame resistance. The absence of chemical action lead to a drastic increase of flame resistance. Both tests were conducted with the same conditions, so all other flow field effects should have been the same. While this is still not sufficient to entirely exclude transport effects of any kind, it seems that we can be secure in concluding that an increase in ion concentration in the outer cone is responsible for the change in flame resistance while cutting.

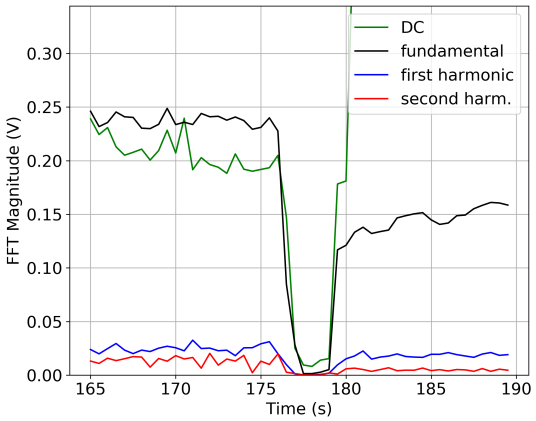

Figure 16: DC, fundamental, and two superharmonics during a successful pierce operation with flow rate 12L/min, f/o ratio 0.78, standoff 6.4mm.

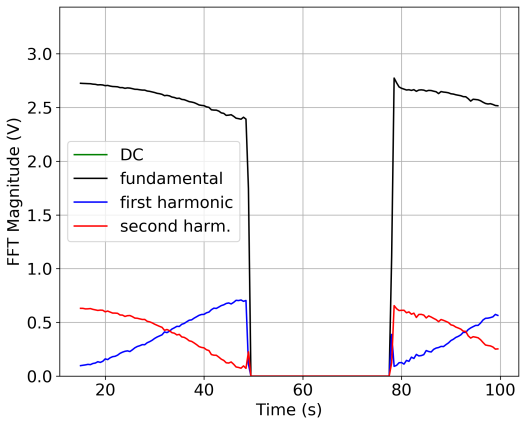

Figure 17: DC, fundamental, and two superharmonics during an unsuccessful pierce operation with flow rate 12L/min, f/o ratio 0.78, standoff 6.4mm.

4.3. Of the sources of unrepeatability

Based on the conclusions of the previous section, it seems obvious that the unsteady aspects of the flame's resistivity during each test are due to the unsteady reaction rate in the cut. The spray of molten metal and metal oxides from the kerf can be seen to pulsate during a typical operation, so it would stand to reason that there may be corresponding pulsations in the ion concentrations in the flame. Furthermore, since the amplitude of the resistance "noise" did not appear to scale with the standoff, it seems that these phenomena do not impact the entire flame, but only the plasma in the vicinity of the work.

Figure 13 shows about ±2.5kΩ of scatter in the mean signal across all tests, and Figure 12 shows a similar magnitude of variation over the course of each test. Since the measurement is insufficiently sensitive to the cutting oxygen pressure and the fuel oxygen ratio to account for the scatter in Figure 13, it is tempting to suggest that these unsteady phenomena alone are to blame for scatter in the height data. However, the unsteady aspects occur over time scales of 1 to 10 seconds and should be well filtered by computing a mean over a 12-inch cut, so they are not a satisfactory explanation. Were we to suppose that the scatter is due to motion of the plate during the preheat process prior to a cut, a 2.5kΩ deviation in resistance would correspond to a ±0.9mm (0.035in) motion of the plate. This is consistent in magnitude to the motions measured by calipers after cuts, and seems a reasonable amount of deflection for a cantilevered plate being heated.

4.4. On the application of these findings

The system under study is likely to be used at standoffs around 3.8mm (0.15in). There, we have confidence in the fits provided in Table 1, so that the standoff could be inferred from a time-averaged resistance measurement to within ±0.7mm (0.028in).

Were the abrupt change in flame conductivity during pierce used to infer the success of the operation, this may constitute the first such sensor to be commercially successful in the endeavor. Infrared sensors that observe the plate radiation are not fast enough to respond to a failed cut and suffer from material-dependent calibrations, while the electrical repercussions to chemical action at the plate surface are nearly immediate at these time scales.

5. Conclusions

- The electrical resistance of the oxyfuel cutting flame under study reduces from 7.8kΩ/mm (200kΩ/in) in preheat to 2.8±0.4kΩ/mm (71±11kΩ/in) while cutting.
- When cutting is initated, the plasma resistivity is reduced by roughly a factor of 3 due to electrons liberated in chemical action at the work.
- Loss of cut, ignition, and failed ignition events have clear electrical signatures in the second (ohmic) and third (work saturation) regimes.
- Mean flame resistance can be related to the standoff distance to within roughly ±0.7mm (.028in) in the region of interest.
- Scatter in the height data is primarily due to motion of the plate during test.
- Tests exhibited unsteady variations in ohmic regime resistance roughly 3kΩ in amplitude that did not scale with the standoff distance.

6. Acknowledgements

This work was performed in part thanks to a donation of steel from Curry Rail of Hollidaysburg, PA; and thanks in part to support from IHT Automation GmbH.

References

[1] C. Martin, C. Leonard, J. VonFricken, A study of the electrical characteristics of an oxyfuel flame, Experimental Thermal and Fluid Science 88 (2017) 65–72. doi:10.1016/j.expthermflusci.2017.05.010.

[2] C. R. Martin, A study of ion currents in an oxyfuel flame due to work surface chemical action, Experimental Thermal and Fluid Science 98 (2018) 239–250. doi:10.1016/j.expthermflusci.2018.06.003.

[3] E. A. Mason, E. W. McDaniel, Transport Properties of Ions in Gases, John Wiley & Sons, New York, 1988.

[4] J. Lawton, F. J. Weinberg, Electrical aspects of combustion, Oxford: Clarendon Press, 1969.

[5] A. B. Fialkov, Investigations on ions in flames, Progress in Energy and Combustion Science 23 (1997) 399–528.

[6] J. Deckers, A. Van Tiggelen, Ion identification in flames, in: Seventh Symposium on Combustion, Vol. 7, Combustion Institute, 1958, pp. 254–255.

[7] H. F. Calcote, Ion production and recombination in flames, in: Eighth Symposium on Combustion, Vol. 8, Combustion Institute, 1961, pp. 184–199.

[8] H. F. Calcote, Mechanisms for formation of ions in flames, Combustion and Flame 1 (4) (1957) 385–403.

[9] D. Bradley, S. M. A. Ibrahim, Determination of positive-ion mobilities and collision cross sections in flame gases using electrostatic probes, Journal of Physics D: Applied Physics 7 (1974) 1377–1390.

[10] F. Bisetti, M. E. Morsli, Calculation and analysis of the mobility and diffusion coefficient of thermal electrons in methane/air premixed flames, Combustion and Flame 159 (2012) 3518–3521. doi:10.1016/j.combustflame.2012.08.002.

[11] J. Hu, B. Rivin, E. Sher, The effect of an electric field on the shape of co-flowing and candle-type methane-air flames, Experimental and Thermal Fluid Science 21 (2000) 124–133.

[12] M. Belhi, P. Domingo, P. Vervisch, Direct numerical simulation of the effect of an electric field on flame stability, Combustion and Flame 157 (2010) 2286–2297.

[13] R. Rao, D. Honnery, A simplified mechanism for the prediction of the ion current during methane oxidation in engine-like conditions, Combustion and Flame 162 (2015) 2928 – 2936.

[14] Y. Xiong, D. G. Park, L. B. Jik, C. S. Ho, C. M. Suk, Dc field response of one-dimensional flames using an ionized layer model, Combustion and Flame 163 (2016) 317–325.

[15] M. D. Renzo, P. D. Palma, M. D. de Tullio, G. Pascazio, An efficient flamelet progress-variable method for modeling non-premixed flames in weak electric fields, Computers and Fluids 157 (2017) 14–27.

[16] B. T. Chorpening, J. D. Thornton, E. D. Huckaby, K. J. Benson, Combustion oscillation monitoring using flame ionization in a turbulent premixed combustor, in: Proceedings of the ASME, Vol. 129, 2007, pp. 352–357.

[17] F. Li, L. Xu, M. Du, L. Yang, Z. Cao, Ion current sensing-based lean blowout detection for a pulse combustor, Combustion and Flame 176 (2017) 263–271.

[18] W. G. Rado, Characteristics of a plasma generated by combustion in a spark ignition engine, Journal of Applied Physics 46 (1974) 2468–2474.

[19] N. Henein, W. Bryzik, A. Abdel-Rehim, A. Gupta, Characteristics of ion current signals in compression ignition and spark ignition engines, SAE International Journal of Engines 3 (1) (2010) 260–281.

[20] T. Badawy, A. Shrestha, N. Henein, Detection of combustion resonance using an ion current sensor in diesel engines, ASME Journal of Engineering for Gas Turbines and Power 134 (2012) 052802–1–9.

[21] R. Rao, D. Honnery, A study of the relationship between NOx and the ion current in a direct-injection diesel engine, Combustion and Flame 176 (2017) 309–317.

[22] A. Jones, Flame failure detection and modern boilers, Journal of Physics E: Scientific Instruments 21 (1988) 921–928.

[23] E. P. Mierzwinski, Integrated furnace control, IEEE Transactions on Industry Applications 27 (2) (1991) 257–261.

[24] F. Weinberg, D. Dunn-Rankin, F. Carleton, S. Karnani, C. Markides, M. Zhai, Electrical aspects of flame quenching, in: Proceedings of the Combustion Institute, Vol. 34, 2013, pp. 3295–3301, doi:10.1016/j.proci.2012.07.007.

[25] N. Speelman, M. Kiefer, D. Markus, U. Maas, L. de Goey, J. van Oijen, Validation of a novel numerical model for the electrical currents in burner-stabilized methane-air flames, in: Proceedings of the Combustion Institute, Vol. 35, 2015, pp. 847–854.

[26] C. Martin, Mechanized oxyfuel control using ion current sensing, The Welding Journal 96 (5) (2017) 154–162.

[27] C. Martin, Replacing mechanized oxyfuel cutting sensors with ion current sensing, in: Proceedings of the ASME 2017 Manufacturing Science and Engineering Conference, Los Angeles, USA, 2017, pp. MSEC2017–2789.

[28] C. Martin, Electrical signatures for chemical action at the work surface in an oxyfuel flame, in: Proceedings of the ASME 2018 Manufacturing Science and Engineering Conference, College Station, TX, 2018, pp. MSEC2018–6354.

[29] T. Kinbra, H. Ikegami, On the positive and negative ions in diffusion flames, Combustion and Flame 1 (2) (1957) 199–256.

[30] S. B. Pope, Turbulent Flows, 9th Edition, Cambridge University Press, New York, 2011.